# Sequential artificial light–harvesting system based on metallacycle for sensitive detection of biothiols

Dengqing Zhang*, Bei Jiang, Jie Yang, Senkun Liu, Xiang Yang, Ke Ma, Xiaojuan Yuan, Lingyan Liu, Tao Yi

State Key Laboratory for Modification of Chemical Fibers and Polymer Materials, College of Chemistry and Chemical Engineering, Donghua University, Shanghai 201620, P. R. China, E-mail: dqzhang@dhu.edu.cn

## Table of contents

## 1. General information

All reagents and solvents were commercially available and used without further purification. $^{1}H$ NMR and $^{13}C$ NMR spectra were recorded in $CDCl_3$ or $CD_3COCD_3$ on Bruker Model Avance DMX 400 (400 MHz) or Bruker Model Avance DMX 600 (600 MHz). Absorption spectra were recorded on a model TU-1901 spectrophotometer (PERSEE). The fluorescence spectra and lifetimes were recorded on a Horiba Fluoro Max+ spectrofluorometer. The fluorescence quantum yields were measured on a FLS1000 with the integrating sphere. Transmission electron microscopy (TEM) images were carried out on a JEOL JEM-2100 instrument. Dynamic light scattering (DLS) measurements were performed at a Malvern Instrument. Zeta-potential measurements were performed on a Zetasizer Nano Z apparatus at 298 K. ESI-TOF-mass spectrum was recorded on a Micromass Quattro II triple-quadrupole mass spectrometer using electrospray ionization with a MassLynx operating system.

The ligand **L2** were synthesized according to the reported literature.[1]

## 2. Determination method in human serums

Two commercial biothiol kits, human total thiol ELISA kit (Enzyme linked immunosorbent assay, from CoiboBio Shanghai, China) and total sulfydryl group content assay kit (Ellman method, from Boxbio Beijing, China), were employed as standard methods for total thiol detection agreement discussion. The test process of the two commercial kits accorded to the provided standard methods. Under the approval of the ethics committee, human serum samples were supplied by Shanghai general hospital (Shanghai, China) and stored at −20 °C. The thawed serums were diluted in PBS to form 80−fold diluted serums for further quantitative analysis without a deproteinization procedure. For the standard curve method, 1600 $\mu$L of PBS, 200 $\mu$L of **MPt1**–ESY–SR101 (100 $\mu$M) in DMSO, and 200 $\mu$L of 80−fold diluted serums were

added in turn to a 5 mL centrifuge tube, with the final diluted concentration of 10 $\mu$M for probe and 800−fold dilution of the original human serum.

## 3. The synthesis of metallacycle MPt1

### 3.1 Synthesis of L1

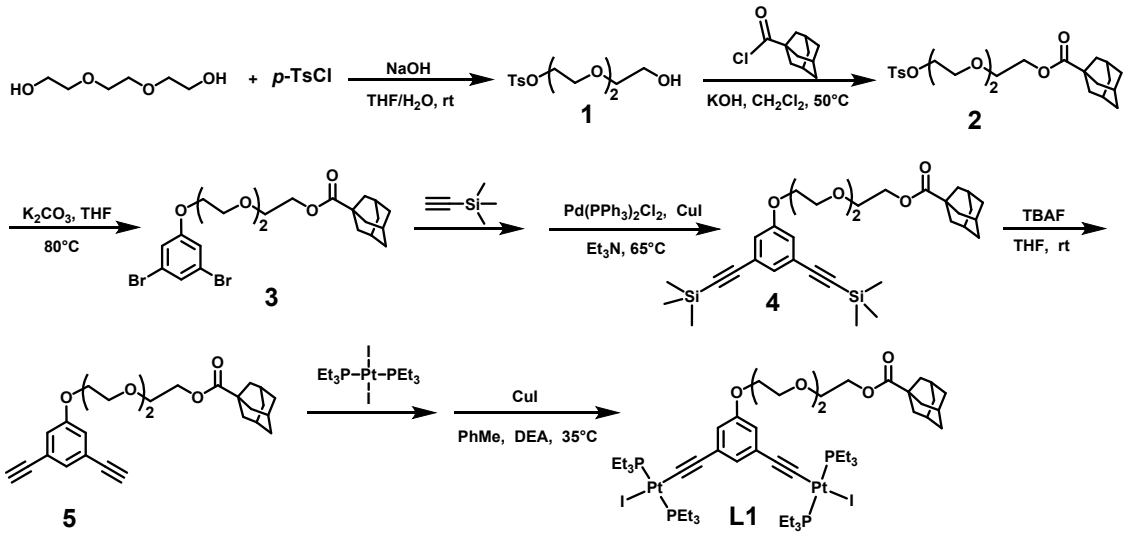


Scheme S1. Synthesis route of **L1**.

#### 3.1.1 Synthesis of 1

**1** was synthesized following the previously reported procedure.[2] Triethylene glycol (826.17 mg, 5.50 mmol) and dry THF (15 mL) were added to an oven-dried round-bottom flask, and then an aqueous solution of NaOH (330.05 mg, 8.25 mmol) (10 mL) was slowly added to the flask. The solution was cooled to 0 °C, and then *p*-toluenesulfonyl chloride (1.36 g, 7.15 mmol) dissolved in THF (25 mL) was added. The solution was allowed to warm to room temperature and stirred for 18 h. The reaction mixture was poured onto an ice/water mixture (100 mL). The organic layer was separated, and the aqueous layer was extracted with dichloromethane (3×50 mL). The combined organic layers were washed twice with water (50 mL), dried with $MgSO_4$ and concentrated in vacuo. The crude product was purified by column chromatography on silica gel (DCM: EA = 3: 1) to give pale yellow oil of **1** (1.14 g, 67.89%).$^1$H NMR

(600 MHz, $CDCl_3$) δ 7.80 (d, *J* = 8.3 Hz, 2H), 7.34 (d, *J* = 8.1 Hz, 2H), 4.18 – 4.14 (m, 2H), 3.70 (q, *J* = 4.9 Hz, 4H), 3.60 (s, 4H), 3.58 – 3.55 (m, 2H), 2.44 (s, 3H). $^{13}C$ NMR (151 MHz, $CDCl_3$) δ 144.92, 132.34, 129.85, 127.87, 72.49, 70.58, 70.09, 69.28, 68.53, 61.47, 21.56.

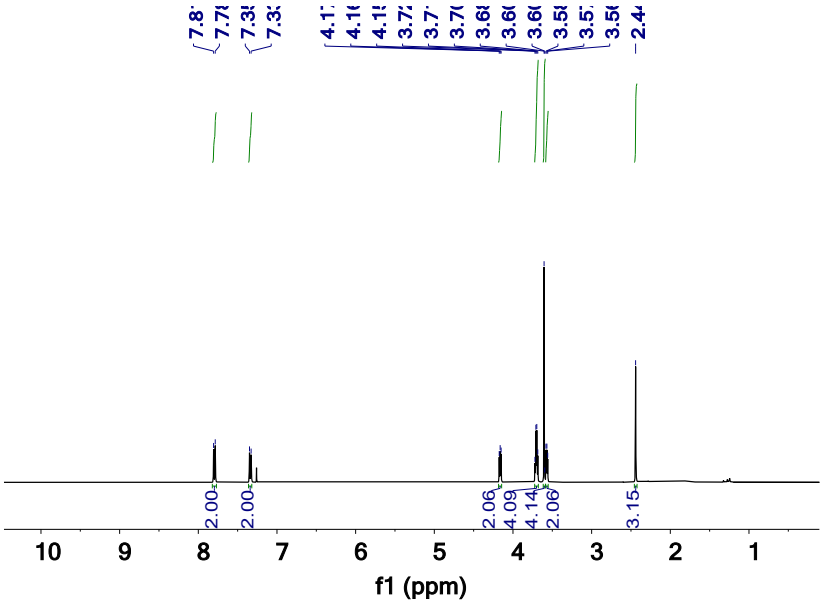


Fig. S1. $^1H$ NMR spectrum of compound **1** (600 MHz, $CDCl_3$, 298 K).

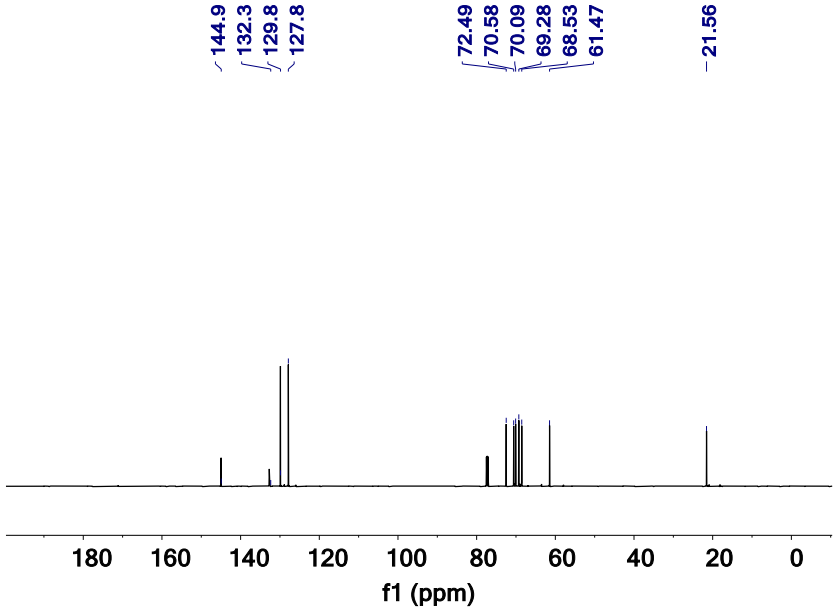


Fig. S2. $^{13}C$ NMR spectrum of **1** (151 MHz, $CDCl_3$, 298 K).

### 3.1.2 Synthesis of 2

**2** was synthesized by following previously reported procedure.[3] The compound **1** (848.8 mg, 2.79 mmol) and potassium hydroxide (558.4 mg, 9.95 mmol) was dissolved

in 20 mL dried $CH_2Cl_2$. The reaction mixture was stirred for 0.5 h. Then, 1-adamantanecarbonyl chloride (693.8 mg, 3.49 mmol) in 5 mL dried $CH_2Cl_2$ was added dropwise at 273 K and then refluxed for 48 h at 323 K under inert atmosphere. The solution was filtrated and concentrated, then passed through a silica gel column (PE: EA = 3:1) to give **2** (637.5 mg, 49.03%). $^1$H NMR (600 MHz, $CDCl_3$) δ 7.83 – 7.77 (m, 2H), 7.37 – 7.32 (m, 2H), 4.21 – 4.12 (m, 4H), 3.71 – 3.68 (m, 2H), 3.66 – 3.63 (m, 2H), 3.58 (s, 4H), 2.44 (s, 3H), 2.03 – 1.97 (m, 3H), 1.88 (d, *J* = 2.9 Hz, 6H), 1.76 – 1.64 (m, 6H). $^{13}$C NMR (151 MHz, CDCl3) δ 177.50, 144.83, 132.93, 129.82, 127.92, 70.70, 70.51, 69.26, 69.20, 68.67, 63.18, 40.61, 38.84, 36.44, 27.87, 21.60. HRMS: m/z Calcd for $C_{24}H_{34}O_7S$ $[M+H]^+$: 467.2095, found 467.2097.

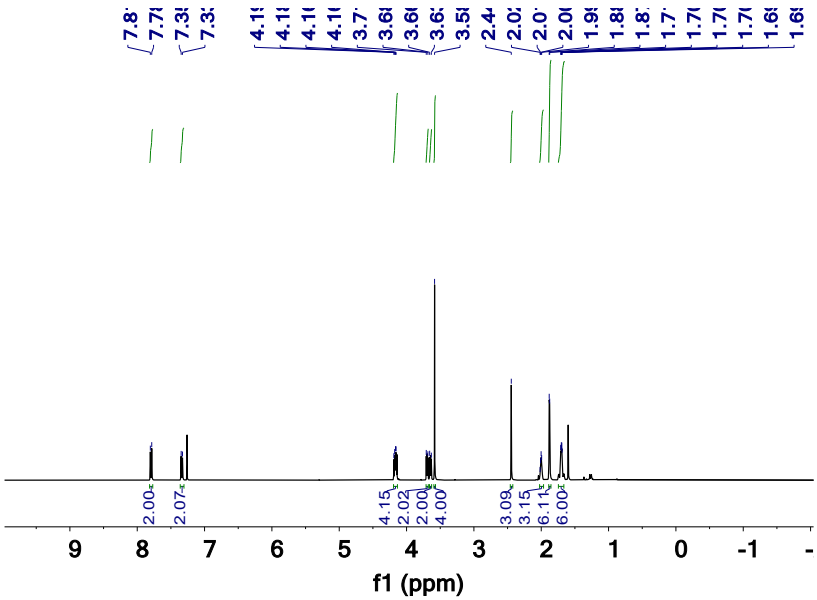


Fig. S3. $^1$H NMR spectrum of compound **2** (600 MHz, $CDCl_3$, 298 K).

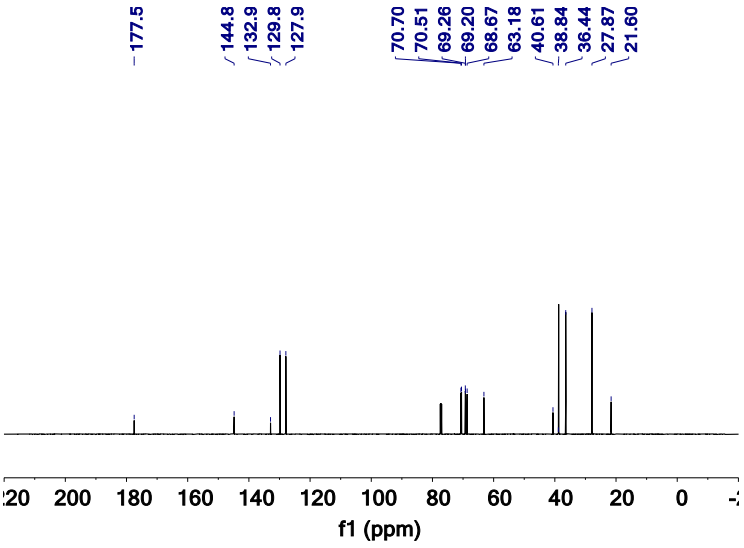

Fig. S4. $^{13}C$ NMR spectrum of **2** (151 MHz, $CDCl_3$, 298 K).

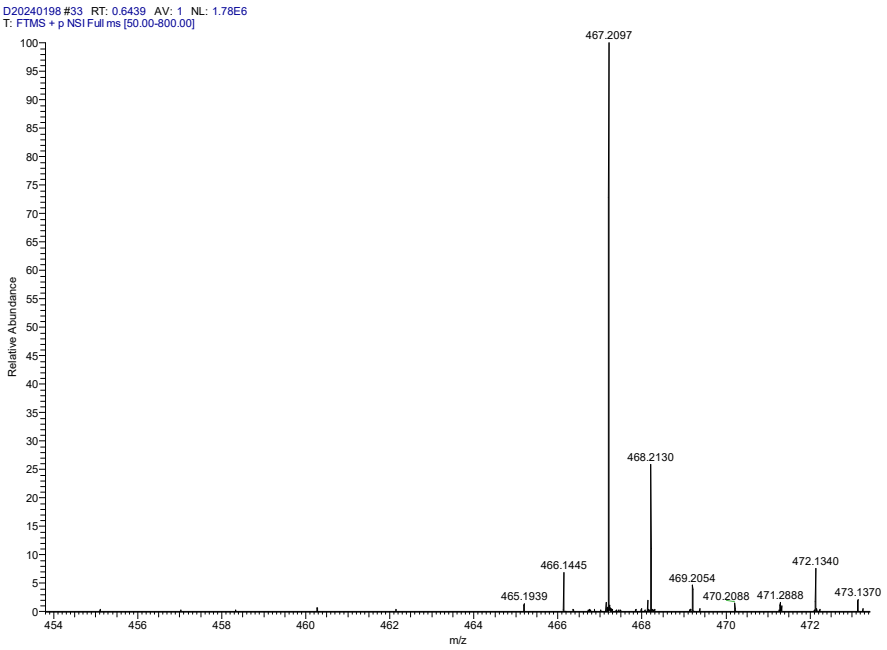


Fig. S5. HRMS spectrum of **2**.

### 3.1.3 Synthesis of 3

3,5-Dibromophenol (524.7 mg, 2.09 mmol), **2** (637.5 mg, 1.37 mmol) and anhydrous potassium carbonate (1.934 g, 13.99 mmol) were added into a 100 mL two-necked flask. Then dry THF (20 mL) was added by syringe. The reaction mixture was heated at 353 K for 36 h under nitrogen, then cooled down to room temperature and the solvents were removed under reduced pressure. The residue was purified by column chromatography on silica gel (PE: EA = 15:1) to afford **3** (595.5 mg, 79.75%) as a pale-yellow oily liquid. $^1H$ NMR (600 MHz, $CDCl_3$) δ 7.24 (d, $J$ = 1.6 Hz, 1H), 7.01 (d, $J$ = 1.7 Hz, 2H), 4.21 (dd, $J$ = 5.7, 4.1 Hz, 2H), 4.09 (dd, $J$ = 5.5, 3.9 Hz, 2H), 3.88 – 3.81 (m, 2H), 3.75 – 3.62 (m, 6H), 1.99 (q, $J$ = 3.3 Hz, 3H), 1.88 (d, $J$ = 2.9 Hz, 6H), 1.75 – 1.64 (m, 6H). $^{13}C$ NMR (151 MHz, $CDCl_3$) δ 177.55, 159.98, 126.57, 123.06, 117.11, 70.92, 70.63, 69.47, 69.31, 68.10, 63.23, 40.67, 38.79, 36.49, 27.93. HRMS: m/z Calcd for $C_{23}H_{30}Br_2O_5$ $[M+H]^+$: 547.0513, found 547.0512.

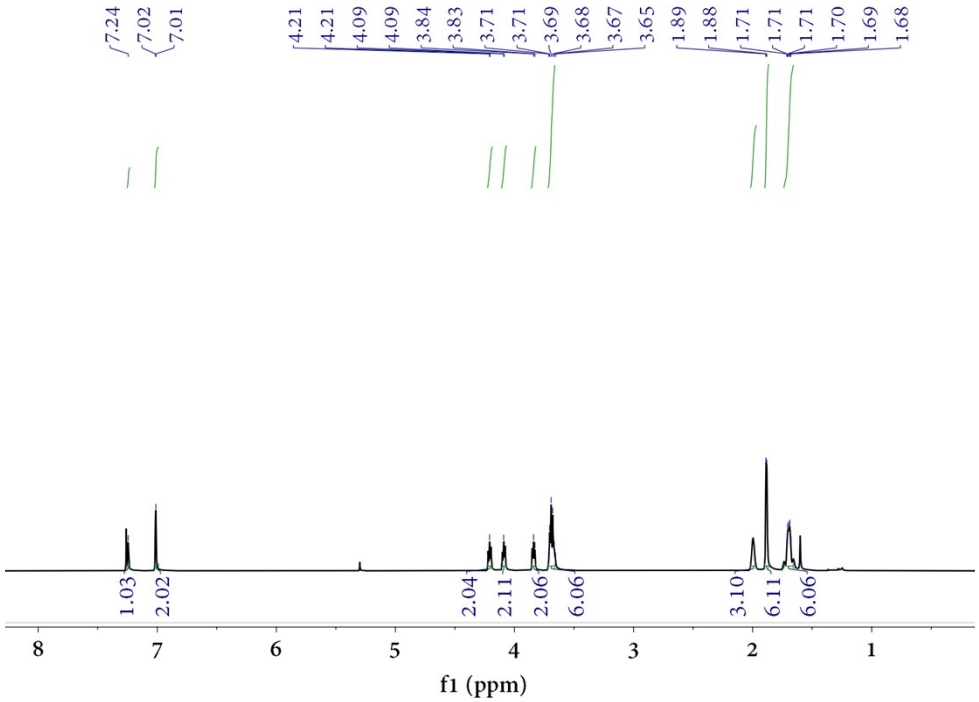


Fig. S6. $^{1}H$ NMR spectrum of compound **3** (600 MHz, $CDCl_3$, 298 K).

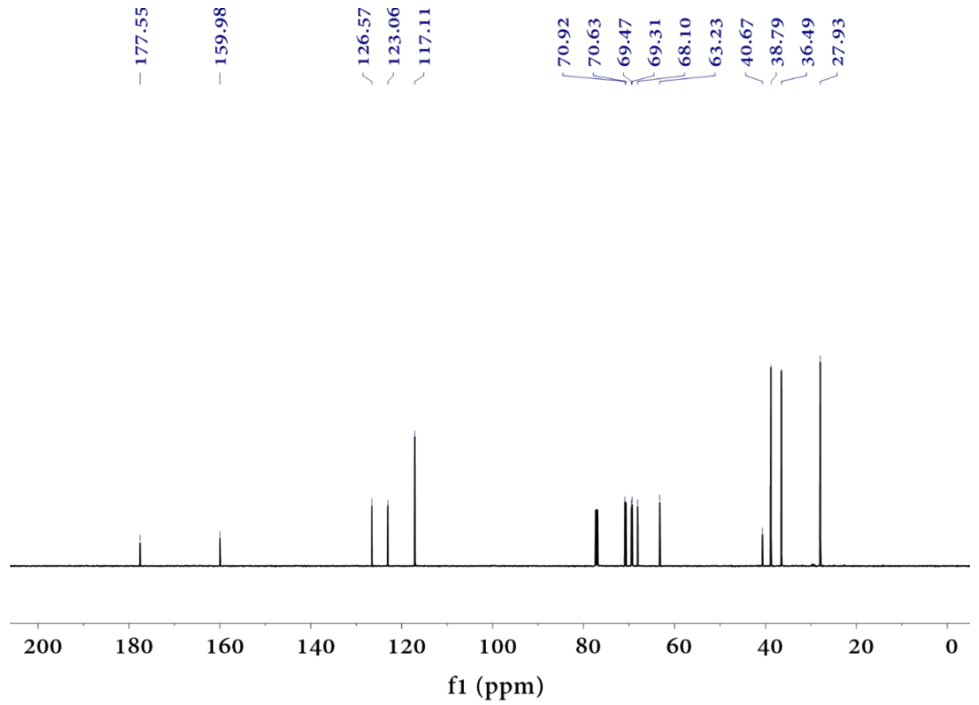


Fig. S7. $^{13}C$ NMR spectrum of **3** (151 MHz, $CDCl_3$, 298 K).

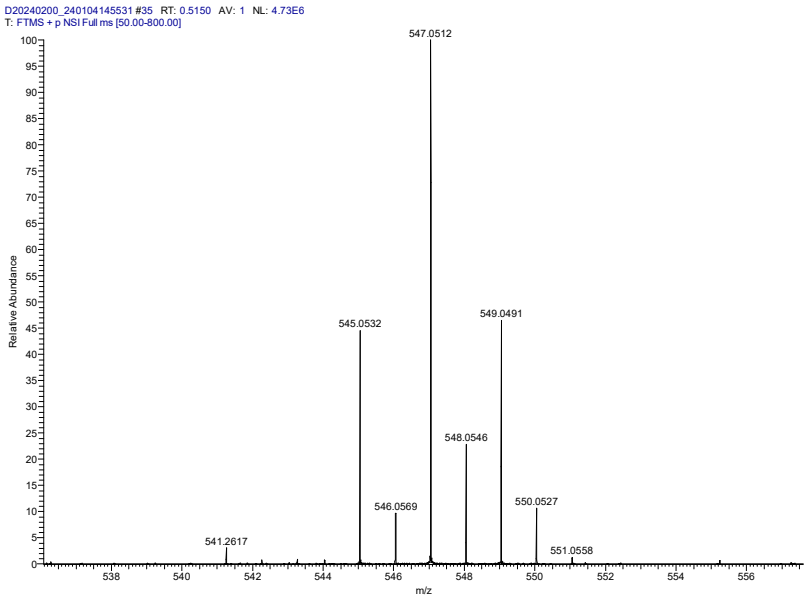


Fig. S8. HRMS spectrum of **3**.

### 3.1.4 Synthesis of 4

To a solution of **3** (590.3 mg, 1.08 mmol) in dry triethylamine (20 mL) were added $Pd(PPh_3)_2Cl_2$ (70.19 mg, 1.04 mmol) and CuI (19.05 mg, 0.108 mmol), the mixture was stirred for 15 min under argon atmosphere. Trimethylsilylacetylene (0.458 mL, 3.239 mmol) was added and the solution was heated to 65 °C and stirred for 16 h. Hexane (10 mL) was added to the reaction mixture, after evaporation of solvent, the residue was purified by column chromatography on silica gel (PE: EA = 10:1) and afforded **4** (373.16 mg, 58.09%) as yellowish oil. $^1$H NMR (600 MHz, $CDCl_3$) δ 7.18 (d, $J$ = 1.5 Hz, 1H), 6.95 (d, $J$ = 1.3 Hz, 2H), 4.23 – 4.19 (m, 2H), 4.09 (t, $J$ = 4.8 Hz, 2H), 3.84 (t, $J$ = 4.8 Hz, 2H), 3.72 – 3.66 (m, 6H), 2.01 – 1.99 (m, 3H), 1.89 (d, $J$ = 2.9 Hz, 6H), 1.70 (q, $J$ = 12.4 Hz, 6H), 0.23 (s, 18H). $^{13}$C NMR (151 MHz, $CDCl_3$) δ 177.54, 158.20, 128.36, 124.23, 118.32, 103.96, 94.67, 70.88, 70.67, 69.59, 69.29, 67.74, 63.24, 40.65, 38.78, 36.49, 27.91, -0.11. HRMS: m/z Calcd for $C_{33}H_{48}O_5Si_2$ $[M+H]^+$: 581.3115, found 581.3112.

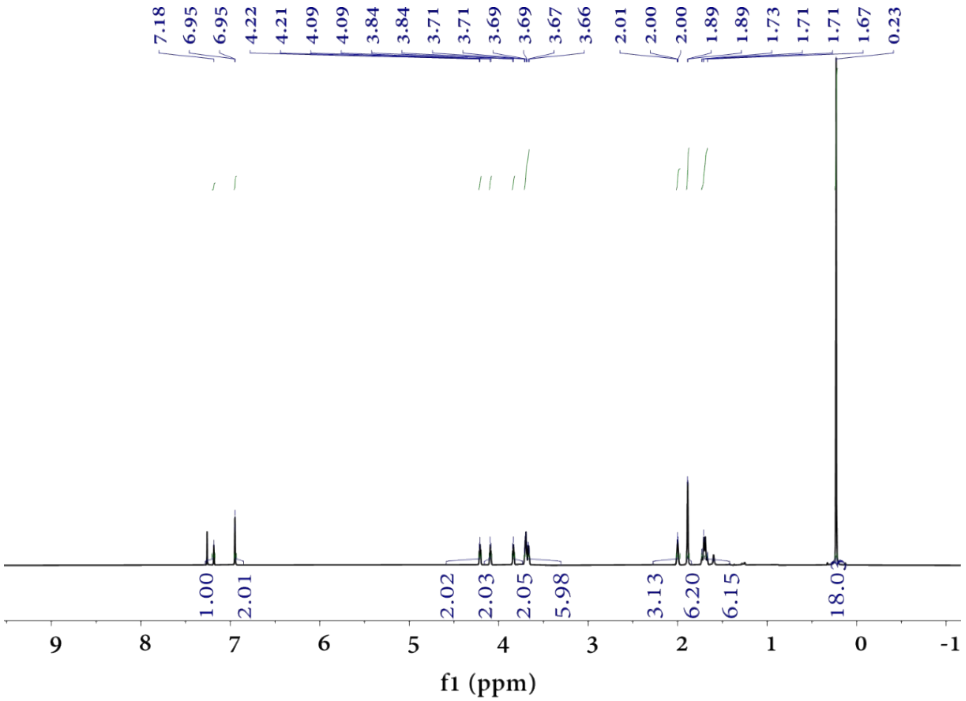


Fig. S9. 1H NMR spectrum of compound **4** (600 MHz, $CDCl_3$, 298 K).

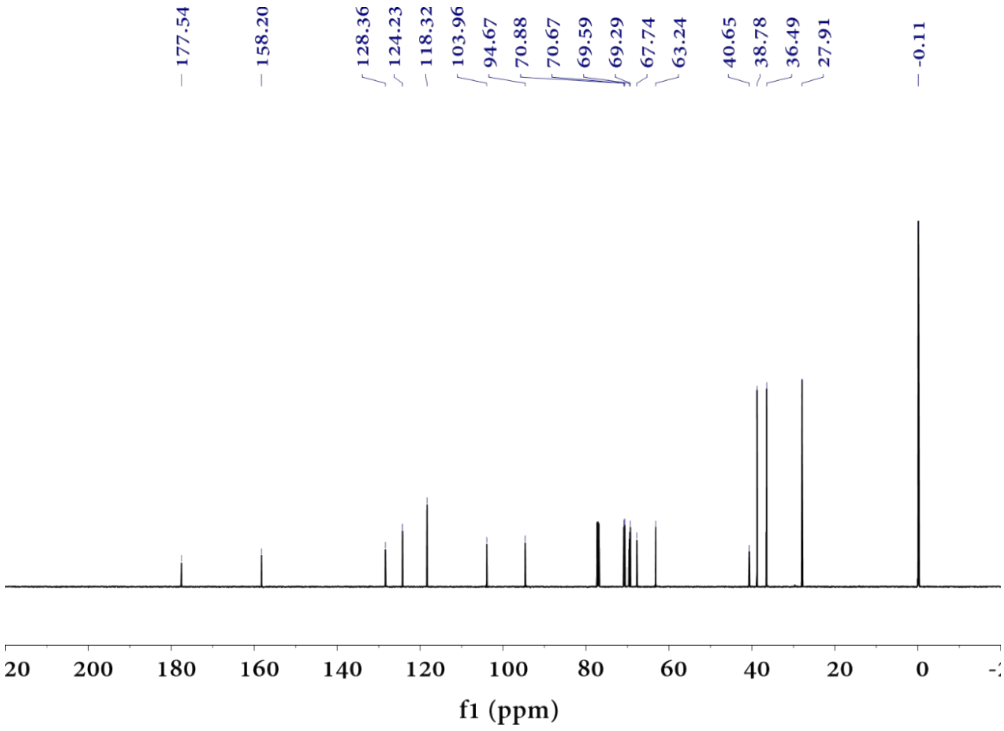


Fig. S10. $^{13}C$ NMR spectrum of **4** (151 MHz, $CDCl_3$, 298 K).

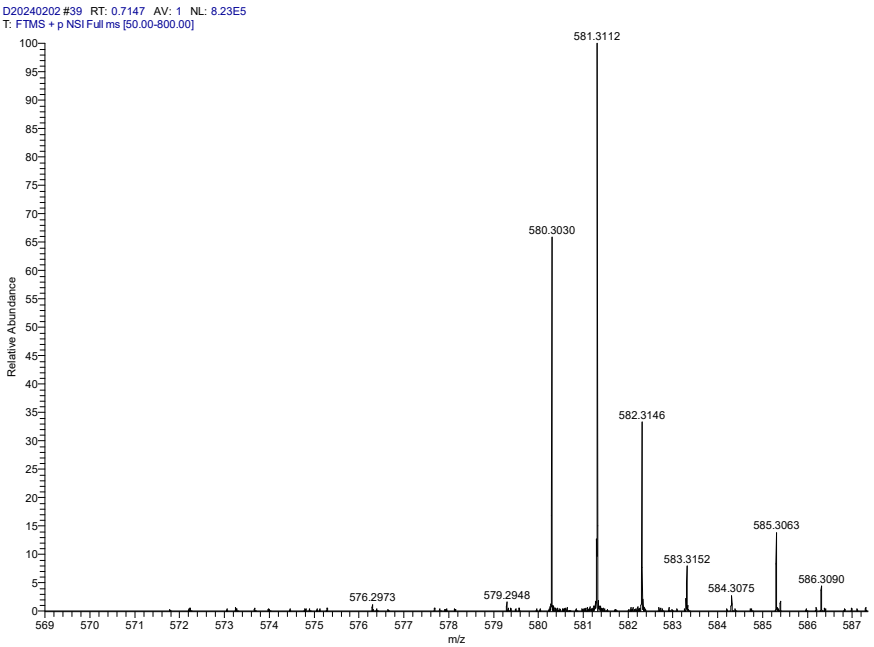


Fig. S11. HRMS spectrum of **4**.

### 3.1.5 Synthesis of 5

A round-bottom flask was charged with **4** (172.2 mg, 0.29 mmol) and THF (15 mL). A solution of tetrabutylammonium fluoride (TBAF) (439.4 mg, 1.68 mmol) in THF (2 mL) was added, and the reaction mixture was stirred for 30 min. Then, water (5 mL) was added and the organic solvents were evaporated. The residue was extracted with dichloromethane, washed with brine and water, and dried over anhydrous sodium sulfate, the solvent was evaporated to give a colorless oil, which was purified by silica gel chromatography (PE: EA = 15: 1) to give **5** (104.6 mg, 80.18%). $^{1}$H NMR (600 MHz, $CDCl_3$) δ 7.21 (d, *J* = 1.4 Hz, 1H), 7.02 (d, *J* = 1.4 Hz, 2H), 4.24 – 4.18 (m, 2H), 4.11 (dd, *J* = 5.7, 3.9 Hz, 2H), 3.85 (dd, *J* = 5.7, 3.9 Hz, 2H), 3.72 – 3.66 (m, 6H), 3.06 (s, 2H), 2.00 (d, *J* = 5.1 Hz, 3H), 1.89 (d, *J* = 2.9 Hz, 6H), 1.70 (dt, *J* = 6.4, 3.1 Hz, 6H). $^{13}$C NMR (151 MHz, $CDCl_3$) δ 177.42, 158.30, 128.29, 124.11, 118.83, 82.47, 78.07, 70.79, 70.58, 69.49, 69.22, 67.25, 62.77, 40.59, 38.73, 36.43, 27.87. HRMS: m/z Calcd for $C_{27}H_{32}O_5$ $[M+H]^+$: 437.2325, found 437.2324.

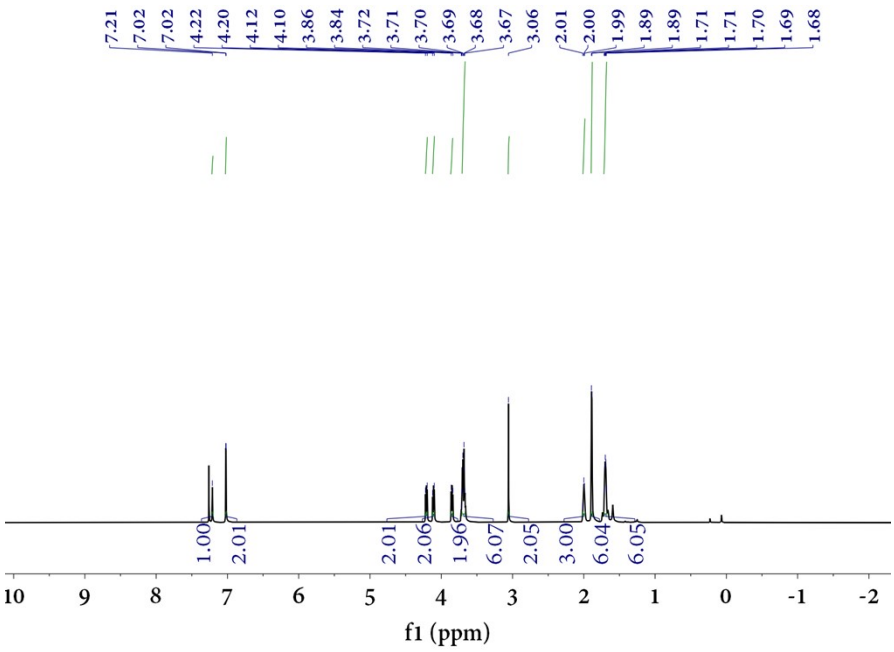


Fig. S12. $^{1}$H NMR spectrum of compound **5** (600 MHz, $CDCl_3$, 298 K).

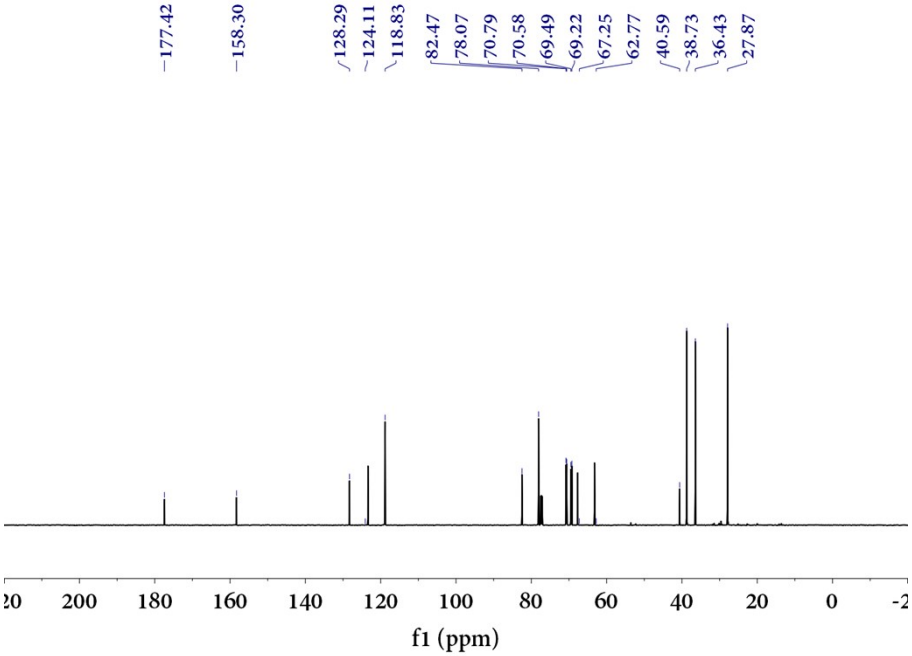


Fig. S13. $^{13}$C NMR spectrum of **5** (151 MHz, $CDCl_3$, 298 K).

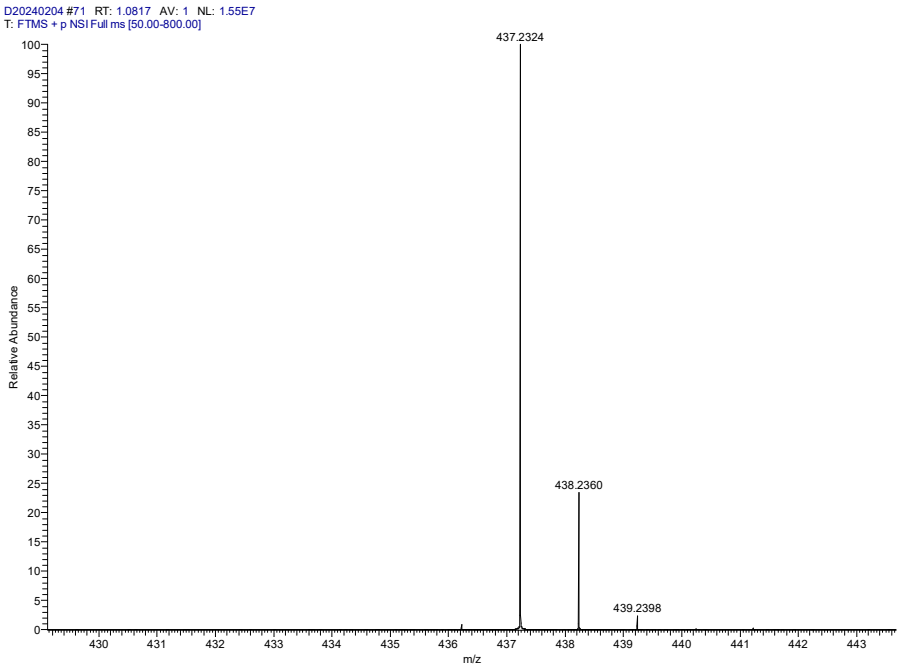


Fig. S14. HRMS spectrum of **5**.

### 3.1.6 Synthesis of L1

To a 50 mL round-bottom Schlenk flask were added **5** (96.4 mg, 0.21 mmol) and *trans*-diiodobis(triethylphosphine)platinum (366.1 mg, 0.53 mmol). Then 10 mL of toluene and 5 mL of dry diethylamine were added under nitrogen. The solution was stirred for 10 min at room temperature before 4 mg of cuprous iodide was added in one portion. After stirring at 308 K for 16 h, the solvent was removed under vacuum, the resulting yellow residue was separated by silica gel column (PE: EA = 3:1) to give a white solid of **L1** (152.4 mg, 45.50%). $^{1}$H NMR (600 MHz, $CDCl_3$) δ 6.81 (s, 1H), 6.66 (s, 2H), 4.20 (t, $J$ = 4.9 Hz, 2H), 4.07 (t, $J$ = 5.0 Hz, 2H), 3.84 (t, $J$ = 4.9 Hz, 2H), 3.69 (dt, $J$ = 9.8, 5.3 Hz, 6H), 2.22 – 2.16 (m, 24H), 1.99 (s, 3H), 1.88 (d, $J$ = 3.0 Hz, 6H), 1.70 – 1.67 (m, 6H), 1.15 (p, $J$ = 7.9 Hz, 36H). $^{13}$C NMR (151 MHz, $CDCl_3$) δ 177.63, 158.24, 129.10, 126.18, 114.35, 99.97, 89.33, 70.82, 70.66, 69.83, 69.31, 67.18, 63.24, 40.68, 38.79, 36.49, 27.92, 16.72, 16.60, 16.48, 8.33.$^{31}$P NMR (162 MHz, $CDCl_3$) δ 8.52(s, $^{195}$Pt satellites, $^{1}J_{Pt\text{-}P}$ = 3489.48 Hz). HRMS: m/z Calcd for $C_{51}H_{90}I_2O_5P_4Pt_2$ $[M+H]^+$: 1552.3224, found 1552.3221.

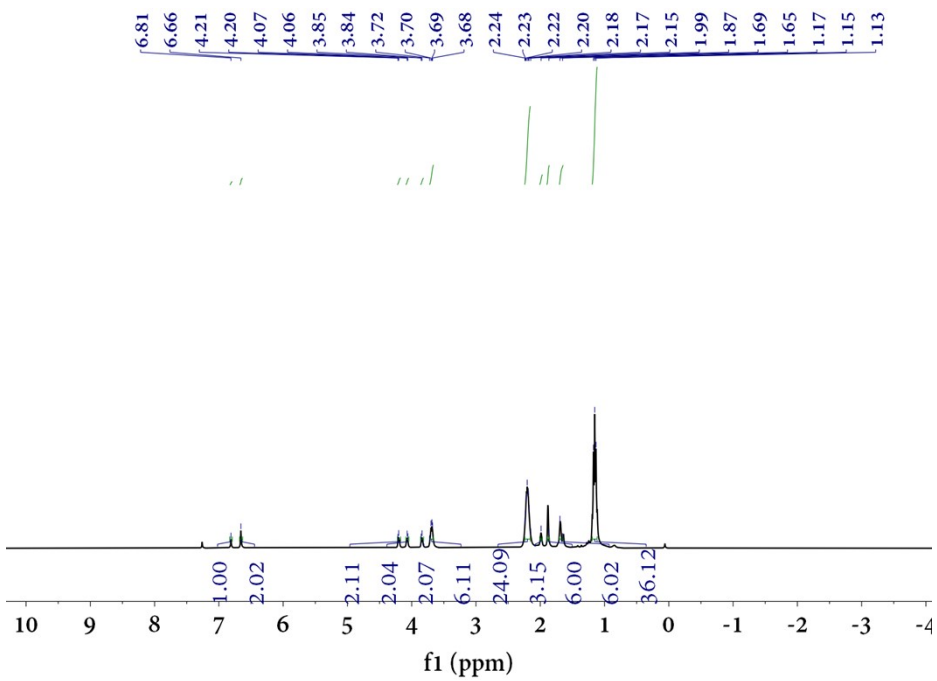


Fig. S15. $^{1}$H NMR spectrum of compound **L1** (600 MHz, $CDCl_3$, 298 K).

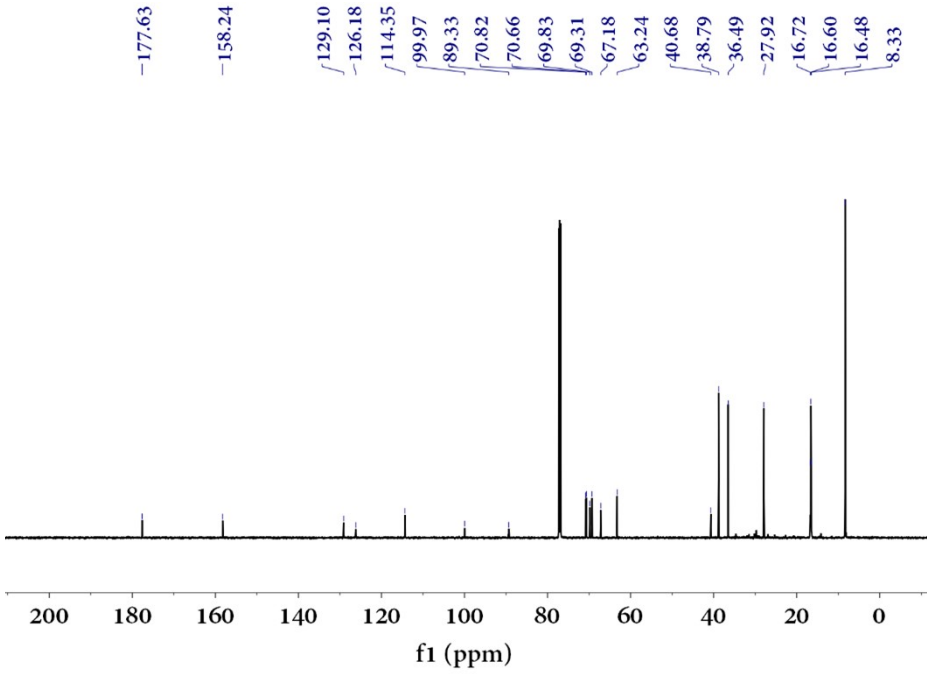


Fig. S16. $^{13}$C NMR spectrum of **L1** (151 MHz, $CDCl_3$, 298 K).

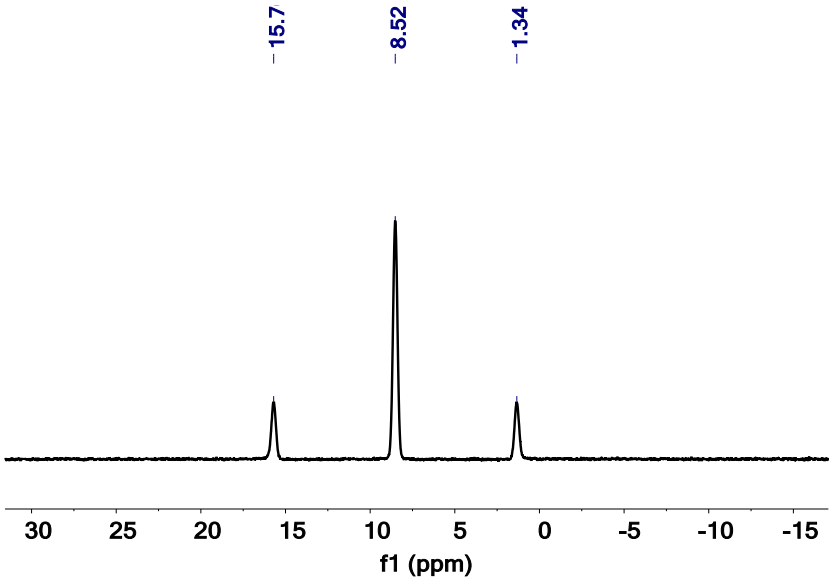


Fig. S17. $^{31}$P NMR spectrum of **L1** (243 MHz, $CDCl_3$, 298 K).

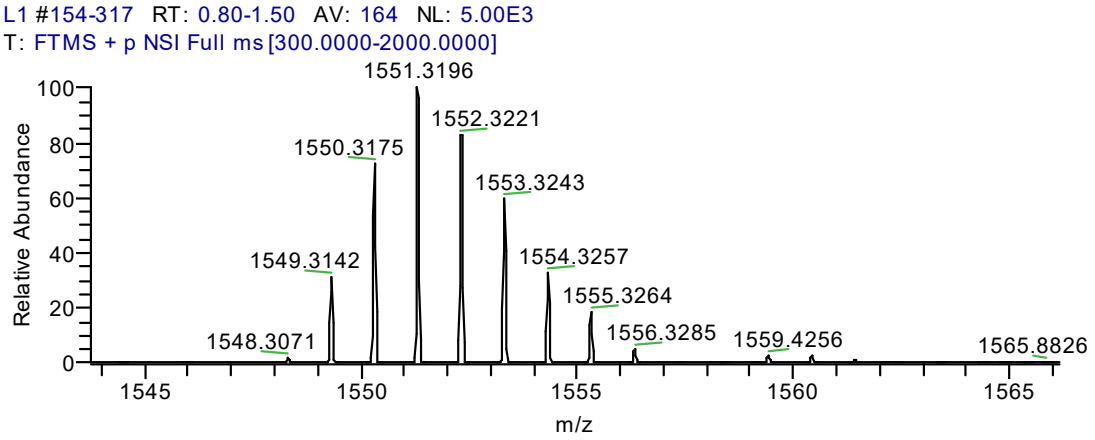


Fig. S18. HRMS spectrum of **L1**.

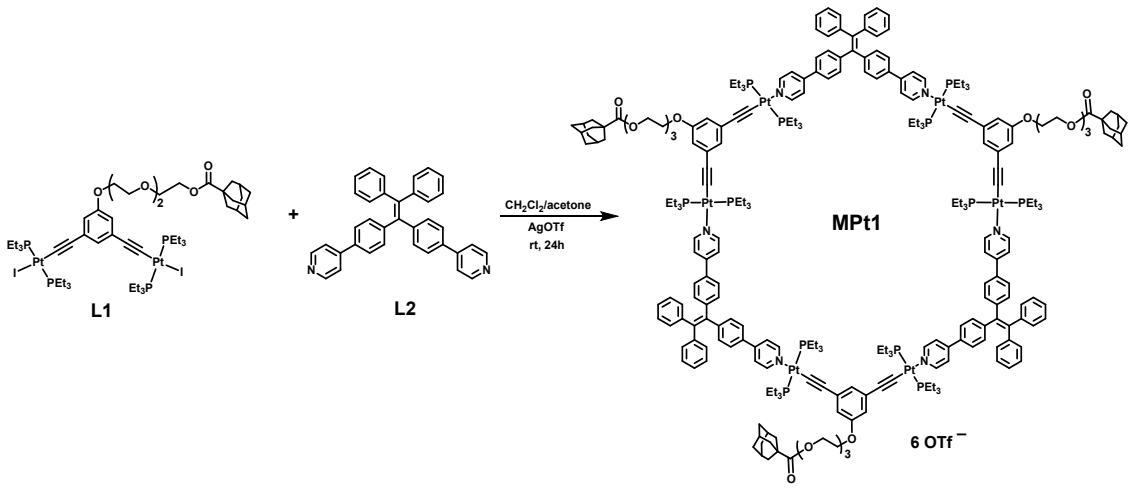

Scheme S2. Synthesis route of **MPt1**.

### 3.2 Synthesis of MPt1

**L1** (15.51 mg, 10.0 $\mu$mol), AgOTf (7.70 mg, 30.0 $\mu$mol) and **L2** (4.86 mg, 10.0 $\mu$mol) were dissolved in the mixture of dichloromethane and acetone (3:1, v/v, 2.0 mL) in a 5 mL glass vial. The reaction mixture was allowed to stir for 24 h at room temperature, and the reaction mixture was centrifuged at 5000 r/h for 15 min. To the resulting homogeneous solution, diethyl ether was added to precipitate the product, which was then isolated and dried under reduced pressure to afford **MPt1** as a yellow–green solid (19. 84 mg). Yield: 97.39%.$^{1}$H NMR (600 MHz, acetone–$d_6$) δ 8.99 (d, $J$ = 6.0 Hz, 12H), 8.14 (s, 12H), 7.84 (s, 12H), 7.31 (d, $J$ = 7.8 Hz, 12H), 7.22 (d, $J$ = 5.9 Hz, 18H),7.16 (d, $J$ = 5.5 Hz, 12H), 7.05 (s, 3H), 6.93 (d, $J$ = 3.5 Hz, 6H), 4.19 – 4.14 (m, 12H), 3.84 (t, $J$ = 4.6 Hz, 6H), 3.68 (t, $J$ = 6.0 Hz, 18H), 2.03 – 1.99 (m, 81H), 1.89 (d, $J$ = 3.0 Hz, 18H), 1.72 (q, $J$ = 12.5 Hz, 18H), 1.25 (q, $J$ = 8.1 Hz, 108H). $^{31}$P NMR (243 MHz, acetone–$d_6$) δ14.67 (s, $^{195}$Pt satellites, $^{1}J_{Pt–P}$ = 2286.63 Hz). ESI–TOF–MS: $C_{267}H_{348}F_{18}N_6O_{33}P_{12}Pt_6S_6$ m/z [M–4OTf]$^{4+}$: 1412.52, [M–5OTf]$^{5+}$: 1100.22.

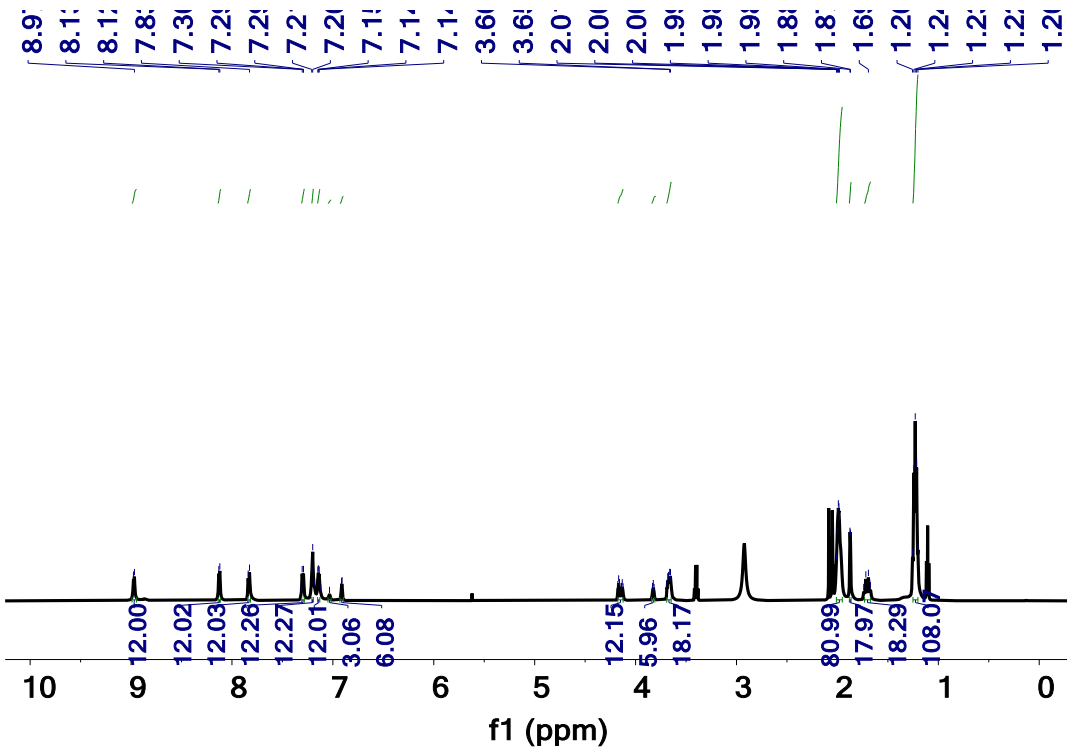


Fig. S19. $^{1}$H NMR spectrum of compound **MPt1** (600 MHz, acetone, 298 K).

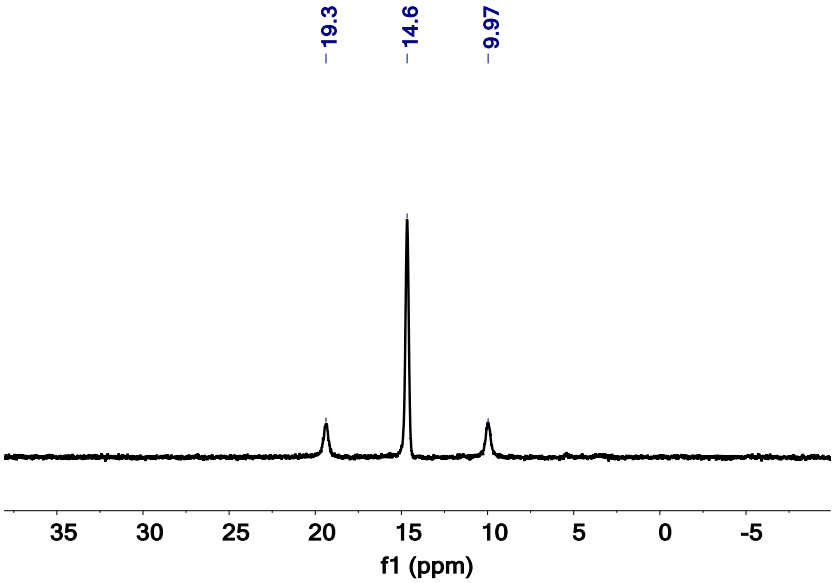


Fig. S20. $^{31}$P NMR spectrum of **MPt1** (243 MHz, acetone, 298 K).

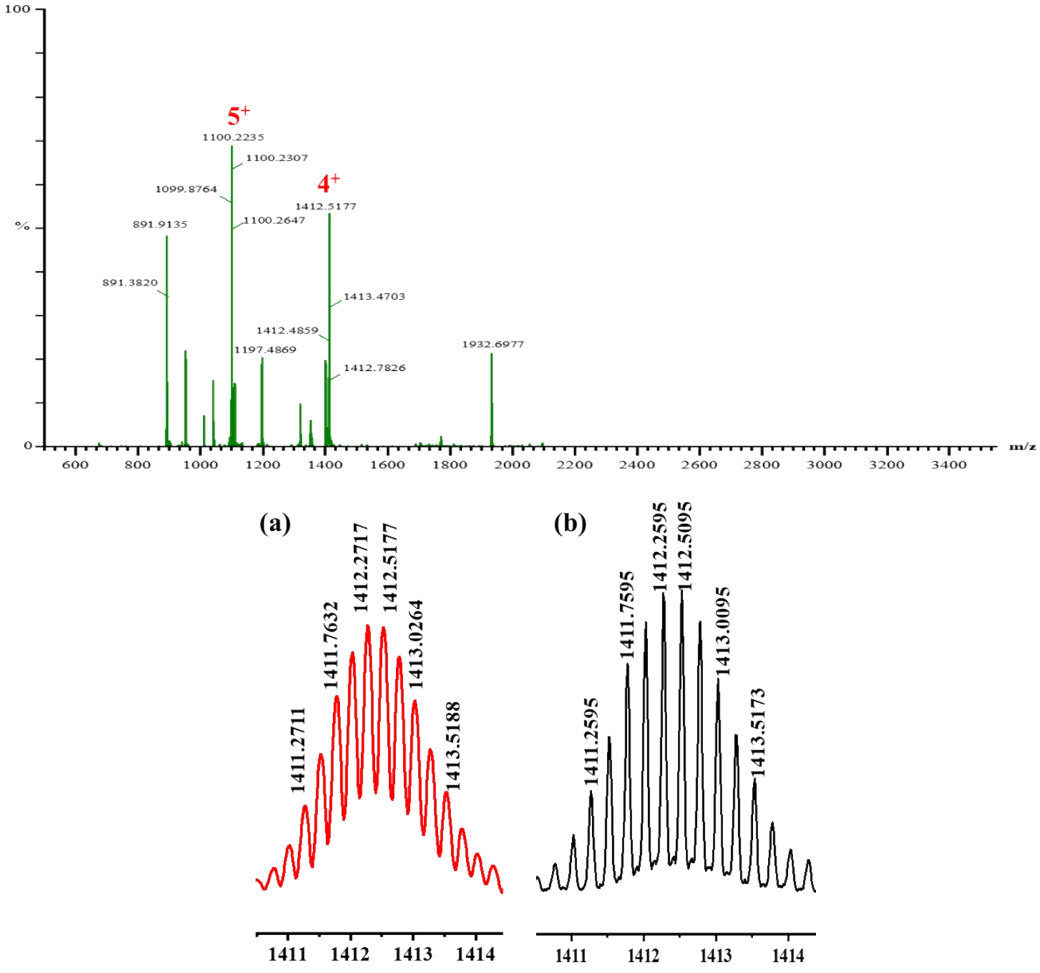


Fig. S21. ESI-TOF-MS of **MPt1**. Experimental (red) and theoretical (black) ESI-TOF-MS spectra of **MPt1** [**MPt1**-4OTf$^-$]$^{4+}$.

## 4. Additional Figures

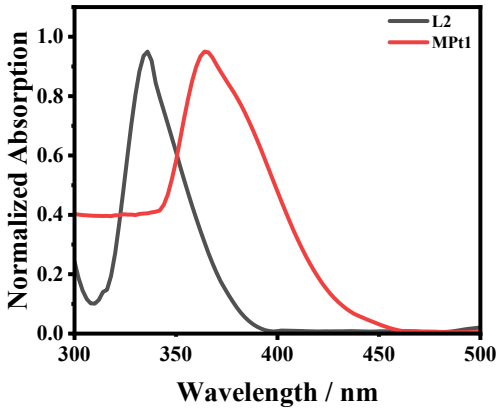


Fig. S22. The absorption spectra of **MPt1**, and **L2** in $CH_3COCH_3$.

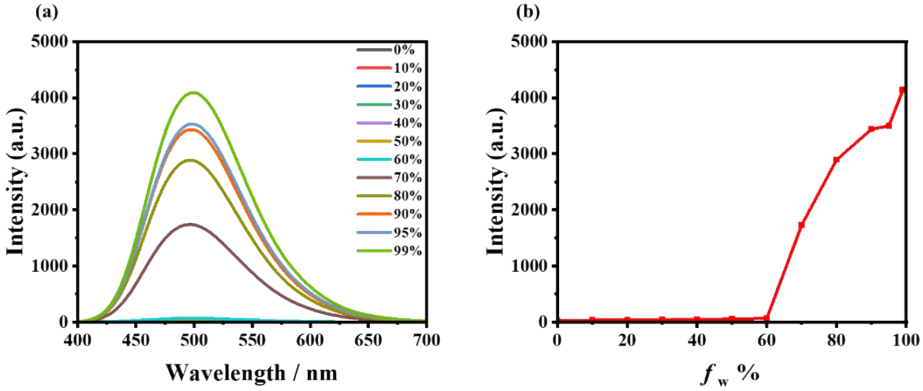


Fig. S23. (a) Fluorescence spectra of **MPt1** in $H_2O/CH_3COCH_3$ mixtures with different water volume fractions ($f_w$, vol %) ($\lambda_{ex}$ = 360 nm). (b) Fluorescence intensity of **MPt1** at 500 nm with various fractions of water from 0 to 99%. All of the fluorescence experiments used 360 nm as the excitation wavelength, [**MPt1**] = 5 μM, slit widths: ex = 2 nm, em = 2nm, 298 K.

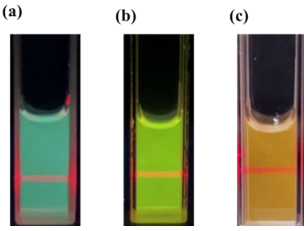


Fig. S24. The Tyndall effect of **MPt1** (a), **MPt1**-ESY (b) and **MPt1**-ESY-SR101 (c) under 365 nm UV light in $H_2O/CH_3COCH_3$ (99:1, v/v), [**MPt1**] = $1.0 \times 10^{-5}$ M, [ESY] = $1.8 \times 10^{-7}$ M, [SR101] = $1.8 \times 10^{-7}$ M.

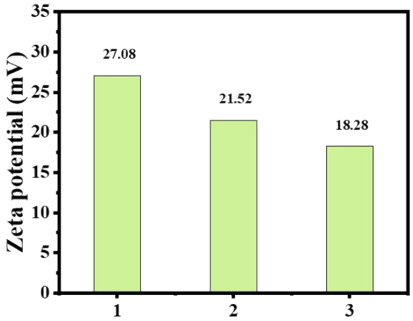


Fig. S25. Zeta potentials of 1: **MPt1**, 2: **MPt1**-ESY (100:1.8), 3: **MPt1**-ESY-SR101 (100:1.8:1.8) in $H_2O/CH_3COCH_3$ (99:1, v/v)

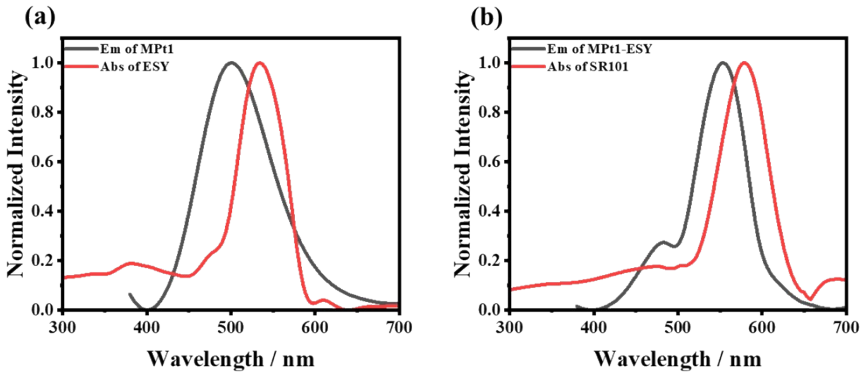


Fig. S26. (a) Normalized absorption spectrum of ESY and emission spectrum of **MPt1**; (b) Normalized absorption spectrum of SR101 and emission spectrum of **MPt1**-ESY (100:1.8). All of the fluorescence experiments used 360 nm as the excitation wavelength, [**MPt1**] = 10 μM, slit widths: ex = 2 nm, em = 2nm, 298 K.

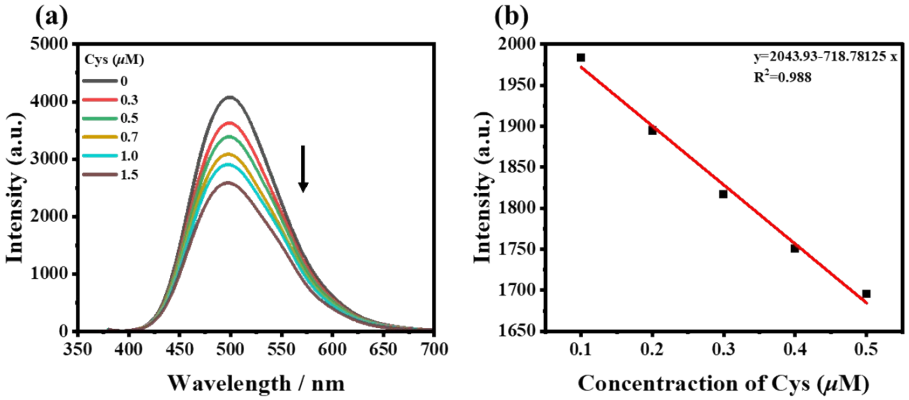


Fig. S27 Fluorescence spectra of **MPt1** (10.0 $\mu$M) upon the addition of increasing concentrations of Cys (a). The emission intensities at 500 nm as a function of Cys concentration (b). Each spectrum was collected in $H_2O/CH_3COCH_3$ (99/1, v/v) with $\lambda_{ex}$= 360 nm, **MPt1** =10.0 $\mu$M, slit widths: ex = 2 nm, em = 2nm, 298 K.

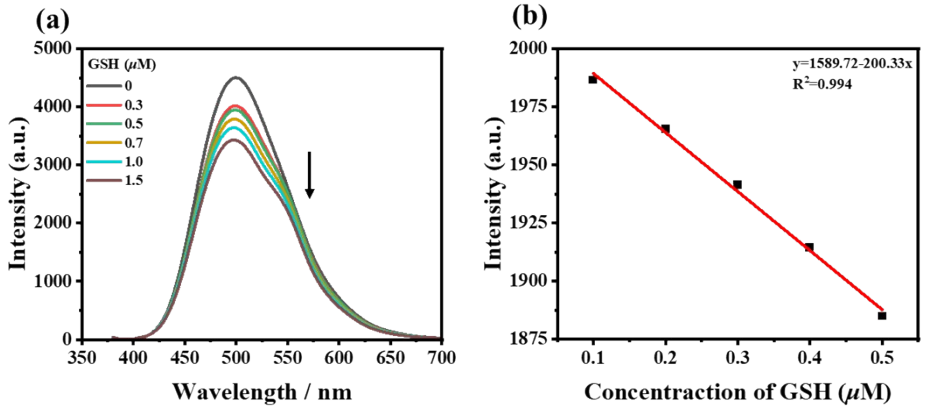


Fig. S28 Fluorescence spectra of **MPt1** (10.0 $\mu$M) upon the addition of increasing concentrations of GSH (0-1.5 $\mu$M) (a). The emission intensities at 500 nm as a function of GSH concentration (b). Each spectrum was collected in $H_2O/CH_3COCH_3$ (99/1, v/v) with $\lambda_{ex}$ = 360 nm. **MPt1** =10.0 $\mu$M, slit widths: ex = 2 nm, em = 2nm, 298 K.

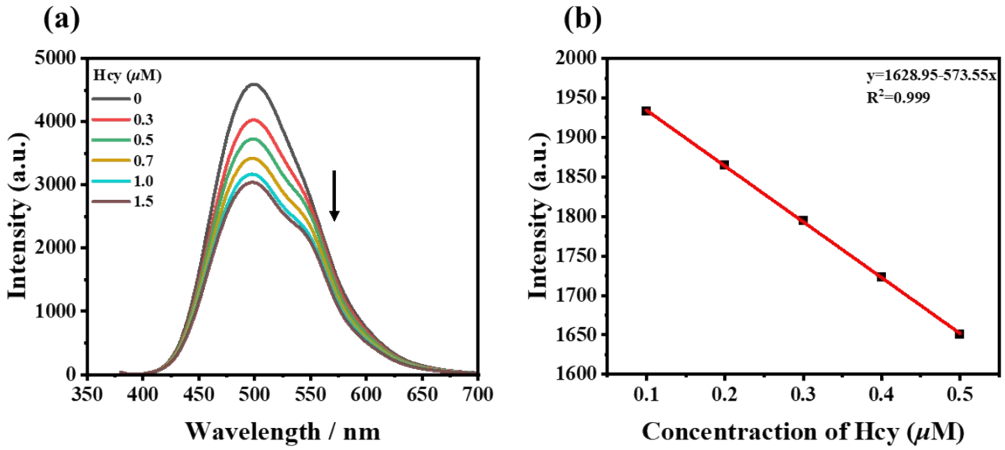


Fig. S29 Fluorescence spectra of **MPt1** (10.0 $\mu$M) upon the addition of increasing concentrations of Hcy (0-1.5 $\mu$M) (a). The emission intensities at 500 nm as a function of Hcy concentration (b). Each spectrum was collected in $H_2O/CH_3COCH_3$ (99/1, v/v) with $\lambda_{ex}$ = 360 nm. **MPt1** =10.0 $\mu$M, slit widths: ex = 2 nm, em = 2nm, 298 K.

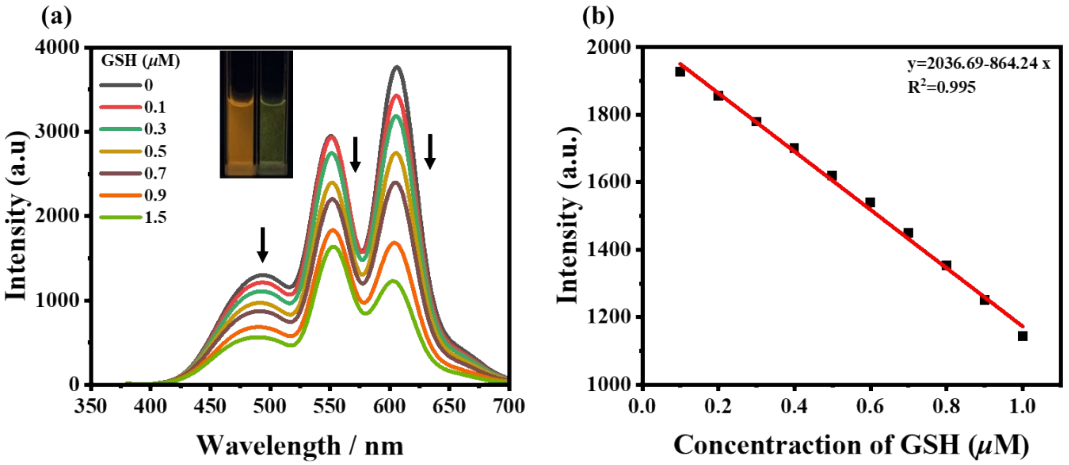


Fig. S30 Fluorescence spectra of **MPt1**-ESY-SR101 (10.0 $\mu$M) upon the addition of increasing concentrations of GSH (a). The inset: fluorescence images of **MPt1**-ESY-SR101 (left) and **MPt1**-ESY-SR101+GSH (right). The emission intensities at 606 nm as a function of GSH concentration (b). Each spectrum was collected in $H_2O$/ $CH_3COCH_3$ (99/1, v/v) with $\lambda_{ex}$ = 360 nm. **MPt1**-ESY-SR101 = 10.0 $\mu$M, GSH =1.5 $\mu$M, slit widths: ex = 2 nm, em = 2nm, 298 K.

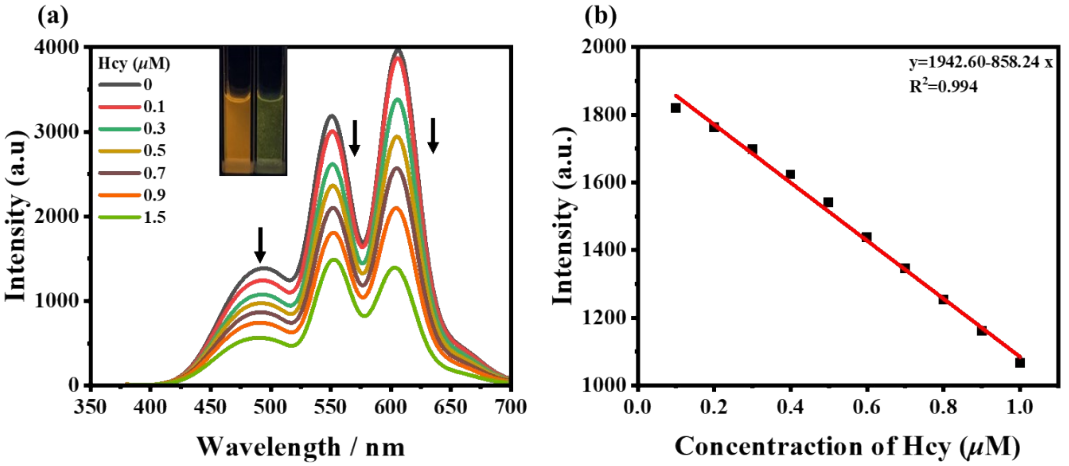


Fig. S31 Fluorescence spectra of **MPt1**-ESY-SR101 (10.0 $\mu$M) upon the addition of increasing concentrations of Hcy (a). The inset: fluorescence images of **MPt1**-ESY-SR101 (left) and **MPt1**-ESY-SR101+Hcy (right). The emission intensities at 606 nm as a function of Hcy concentration (b). Each spectrum was collected in $H_2O/CH_3COCH_3$ (99/1, v/v) with $\lambda_{ex}$ = 360 nm. **MPt1**-ESY-SR101 = 10.0 $\mu$M, Hcy = 1.5 $\mu$M, slit widths: ex = 2 nm, em = 2nm, 298 K.

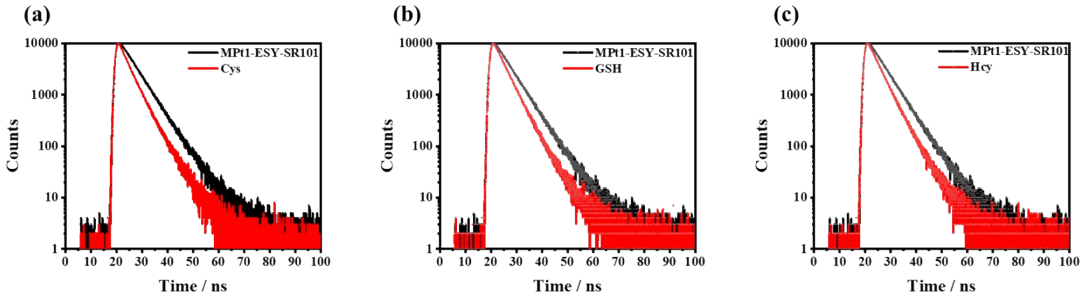


Fig. S32 Fluorescence decay kinetic traces of (a) **MPt1**–ESY–SR101 and **MPt1**–ESY–SR101+Cys recorded at λ = 606 nm, (b) **MPt1**–ESY–SR101 and **MPt1**–ESY–SR101+GSH recorded at λ = 606 nm and (c) **MPt1**–ESY–SR101 and **MPt1**–ESY–SR101+Hcy recorded at λ = 606 nm. The excitation wavelength for all fluorescence experiments was 360 nm. [**MPt1**-ESY-SR101] =10.0 $\mu$M, [Cys] =1.5 $\mu$M, [GSH] =1.5 $\mu$M, [Hcy] =1.5 $\mu$M, slit widths: ex = 2 nm, em = 2nm, 298 K.

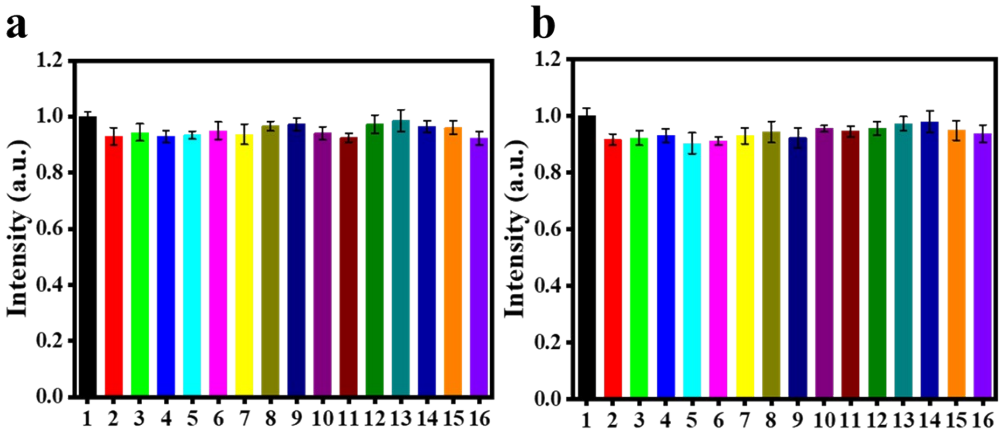


Fig. S33: The anti-interference test of probe **MPt1**-ESY-SR101 to GSH with other reactive species, cations, anions (a). The anti-interference test of probe **MPt1**-ESY-SR101 to Hcy with other reactive species, cations, anions (b). Numbers 1-16 represent :1. **MPt1**-ESY-SR101+Cys, 2. Ala, 3. Ser, 4. Gly, 5. Leu, 6. Arg, 7. Pro, 8. Lys, 9. His, 10. $K^{+}$, 11. $Ca^{2+}$,12. $Na^{+}$, 13. $Mg^{2+}$, 14. $Cu^{2+}$,15. $Fe^{3+}$, 16. $Cl^{-}$, respectively. $\lambda_{ex}$ = 360 nm. $\lambda_{em}$ = 606 nm.

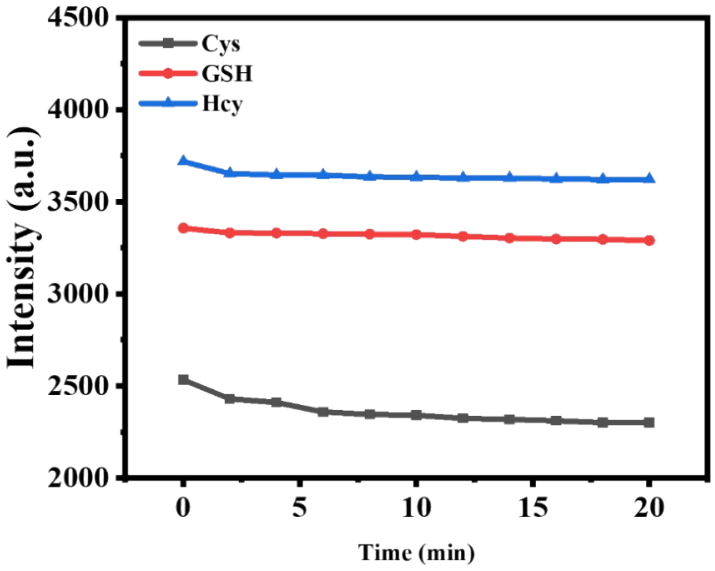


Fig S34. Time-dependent fluorescence intensity changes of **MPt1**-ESY-SR101 (10.0 $\mu$M) in the presence of biothiols (1.5 $\mu$M) at 606nm, $\lambda_{ex}$ = 360 nm.

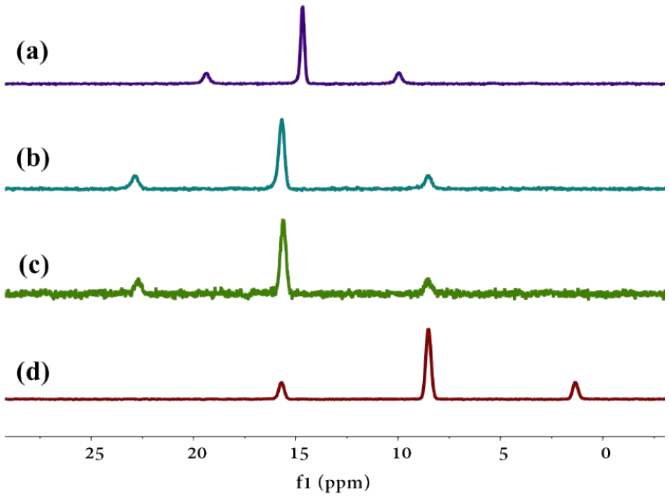


Fig S35. Partial $^{31}P\{1H\}$ NMR spectra (121.4 MHz, acetone-$d_6$) of **MPt1** (a), **MPt1**+Cys (b), **L1**+Cys (c) and **L1** (d).

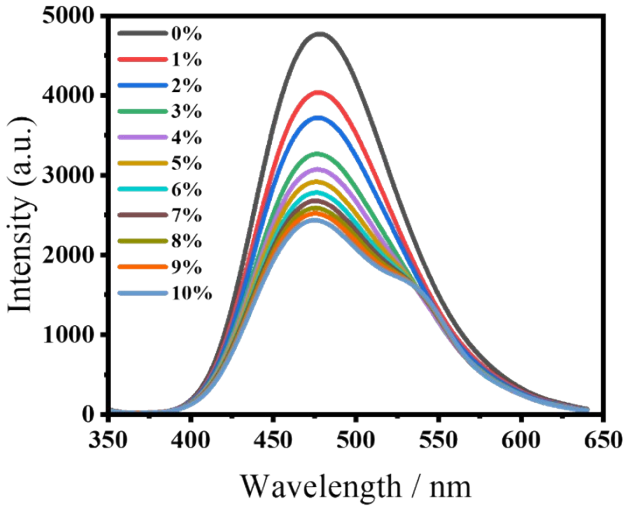


Fig. S36. Fluorescence spectra of **L2** (10 μM) in $H_2O/CH_3COHCH_3$ (99:1, v/v) with varying amounts of **ESY** ($\lambda_{ex}$ = 330 nm), slit widths: ex = 2 nm, em = 2nm, 298 K.

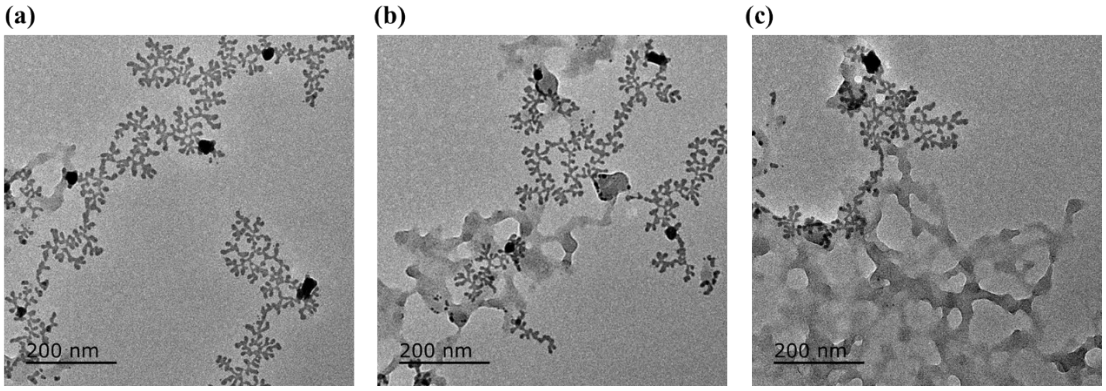


Fig S37. TEM images of **MPt1**-ESY-SR101 assemblies + Cys (a), **MPt1**-ESY-SR101 assemblies + GSH (b), and **MPt1**-ESY-SR101 assemblies + Hcy.

## 5. Experimental procedure and methods

### 5.1 The preparation of the samples

The stock solution of **MPt1** ($1\times10^{-3}$ M, dissolved in $CH_3COCH_3$), ESY ($1\times10^{-5}$ M, dissolved in $H_2O$ /$CH_3COCH_3$, v/v; 99:1), SR101 ($1\times10^{-5}$ M, dissolved in $H_2O$ /$CH_3COCH_3$, v/v; 99:1) were prepared, respectively. **MPt1** assembly was prepared as follows: 20 $\mu$L of **MPt1** stock solution was added into the mixture of water (1980 $\mu$L) under stirring to afford $1\times10^{-5}$ M solution ($H_2O$/ $CH_3COCH_3$, v/v; 99:1). **MPt1**-ESY assembly was prepared as follows: 36 $\mu$L of ESY stock solution was added into 2 mL

of **MPt1** assembly. **MPt1**-ESY-SR101 system was prepared as follows: 36 $\mu$L of SR101 solution was added into 2 mL of **MPt1**-ESY system (100:1.8).

### 5.2 Overlap integral calculation

The calculation of overlap integral, $J(\lambda)$ by using the following relation

$$J(\lambda) = \frac{\int_0^\infty I_D(\lambda)\in_A(\lambda)\lambda^4 d\lambda}{\int_0^\infty I_D(\lambda)d\lambda} \qquad \text{(eq. S1)}$$

Where, $I_D(\lambda)$ = the normalized PL emission intensity of the donor component within the spectral range of $\lambda$ to ($\lambda$+$d\lambda$).

$\varepsilon_A(\lambda)$ = the molar extinction coefficient of the acceptor at wavelength $\lambda$.

### 5.3 Förster distance calculation

Förster distance, $R_0$, which is the specific distance between donor and acceptor for which energy-transfer efficiency is 50%, was calculated by using the following relation.

$$R_0 = 0.211 \times [k^2\, \theta_D\, J(\lambda)/\, \eta^4]^{1/6} \qquad \text{(eq. S2)}$$

Where, $k^2$ = 2/3, $\theta_D$ and $\eta$ are the orientation factor, PLQY of the donor and refractive index of the medium, respectively.

### 5.4 Energy transfer efficiency ($\Phi_{ET}$)

The energy-transfer efficiency ($\Phi_{ET}$) was calculated using equation S3:

$$\Phi_{ET} = 1 - I_{DA}, (\lambda_{ex} = \text{donor})/I_D, (\lambda_{ex} = \text{donor}) \qquad \text{(eq. S3)}$$

For **MPt1**-ESY system, where $I_{DA}$ and $I_D$ are the fluorescence intensities of **MPt1**-ESY assembly (donor and acceptor) and **MPt1** assembly (donor) at 500 nm when excited at 360 nm, respectively. The energy-transfer efficiency ($\Phi_{ET}$) was calculated as 54.82% in $H_2O$/ $CH_3COCH_3$ (99:1; v/v), measured under the condition of [**MPt1**] = 1.0 × $10^{-5}$ M, [ESY] = 1.8 × $10^{-7}$ M, and $\lambda_{ex}$ = 360 nm.

For the **MPt1**-ESY-SR101 system, where $I_{DA}$ and $I_D$ are the fluorescence intensities of **MPt1**-ESY-SR101 assembly (donor and acceptor) and **MPt1**-ESY assembly (donor) at 550 nm when excited at 360 nm, respectively. The energy-transfer

efficiency ($\Phi_{ET}$) was calculated as 56.39% in $H_2O/CH_3COCH_3$ (99:1; v/v), measured under the condition of [**MPt1**] = 1.0 × $10^{-5}$ M, [ESY] = 1.8 × $10^{-7}$ M, [SR101] =1.8 × $10^{-7}$ M, and $\lambda_{ex}$ = 360 nm.

**5.5 Antenna effect (AE)**

The antenna effect (AE) was calculated using equation S4.

Antenna effect = ($I_{DA}$, ($\lambda_{ex}$ = donor) - $I_D$, ($\lambda_{ex}$ = donor))/$I_{DA}$, ($\lambda_{ex}$ = acceptor) (eq. S4)

Where $I_{DA}$, ($\lambda_{ex}$ = donor) and $I_{DA}$, ($\lambda_{ex}$ = acceptor) are the fluorescence intensities of the system with excitation of donor and direct excitation of acceptor, respectively. $I_D$, ($\lambda_{ex}$ = donor) is the fluorescence intensities of the donor.

For **MPt1**-ESY system, where $I_{DA}$, ($\lambda_{ex}$ = donor) and $I_{DA}$, ($\lambda_{ex}$ = acceptor) are the fluorescence intensities at 550 nm with the excitation of the donor at 360 nm and the direct excitation of the acceptor at 525 nm, respectively. $I_D$, ($\lambda_{ex}$ = donor) is the fluorescence intensities at 550 nm of the **MPt1** assembly, which was normalized with the **MPt1**-ESY assembly at 500 nm. The antenna effect value was calculated as 11.42 in $H_2O/CH_3OCH_3$ (99:1, v/v), measured under the condition of [**MPt1**] = 1.0 × $10^{-5}$ M, [ESY] = 1.8 × $10^{-7}$ M, and $\lambda_{ex}$ =360 nm (Fig. S38a).

For **MPt1-ESY-SR101** system, where $I_{DA}$, ($\lambda_{ex}$ = donor) and $I_{DA}$, ($\lambda_{ex}$ = acceptor) are the fluorescence intensities at 606 nm with the excitation of the donor at 360 nm and the direct excitation of the acceptor at 585 nm, respectively. $I_D$, ($\lambda_{ex}$ = donor) is the fluorescence intensities at 606 nm of the **MPt1**-ESY assembly, which was normalized with the **MPt1**-ESY-SR101 assembly at 550 nm. The antenna effect value was calculated as 16.07 in $H_2O/CH_3OCH_3$ (99:1, v/v), measured under the condition of [**MPt1**] = 1.0 × $10^{-5}$ M, [ESY] = 1.8 × $10^{-7}$ M, [SR101] = 1.8 × $10^{-7}$ M, and $\lambda_{ex}$ = 360 nm (Fig. S38b).

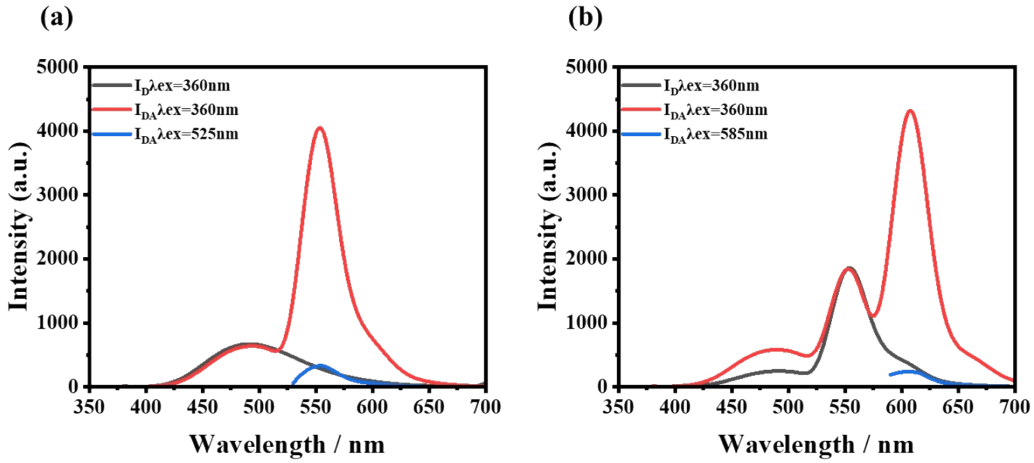


Fig. S38. (a) Fluorescence spectra of **MPt1**-ESY (black line, [**MPt1**] = 1.0 × $10^{-5}$ M, [ESY] = 1.8 × $10^{-7}$ M, $\lambda_{ex}$ = 360 nm), the donor (red line, $\lambda_{ex}$ = 360 nm) and acceptor (blue line, $\lambda_{ex}$ = 525 nm). The fluorescence intensity of **MPt1**-ESY at 500 nm was normalized according to the fluorescence intensity of the donor; (b) Fluorescence spectra of **MPt1**-ESY-SR101 (black line, [**MPt1**] = 1.0 × $10^{-5}$ M, [ESY] = 1.8 × $10^{-7}$ M, [SR101] = 1.8 × $10^{-7}$ M, $\lambda_{ex}$ =360 nm), the donor (red line, $\lambda_{ex}$ = 360 nm) and acceptor (blue line, $\lambda_{ex}$ = 585 nm). The fluorescence intensity of **MPt1**-ESY-SR101 at 550 nm was normalized according to the fluorescence intensity of the donor. All of the fluorescence experiments used 360 nm as the excitation wavelength, [**MPt1**] = 10 μM, slit widths: ex = 2 nm, em = 2nm, 298 K.

## 6. Additional tables

Table S1. Fluorescence lifetimes of **MPt1**, **MPt1**-ESY, **MPt1**-ESY-SR101, assemblies in $H_2O/CH_3OCH_3$ (99:1, v/v).

| Sample | $\tau_1$/ns | Rel% | $\tau_2$/ns | Rel% | A | $\chi^2$ |
|---|---|---|---|---|---|---|
| **MPt1**[a] | 1.41 | 62.83 | 3.18 | 94.31 | 1.688 | 1.204 |
| **MPt1**-ESY[a] | 1.09 | 45.86 | 2.59 | 60.27 | 1.135 | 1.162 |
| **MPt1**-ESY[b] | 1.88 | 63.57 | 7.52 | 94.53 | 1.426 | 1.222 |
| **MPt1**-ESY-SR101[b] | 1.70 | 41.53 | 6.82 | 65.64 | 1.266 | 1.152 |
| **MPt1**-ESY-SR101[c] | 2.20 | 64.28 | 8.80 | 93.70 | 1.507 | 1.199 |
| **MPt1**-ESY-SR101+Cys[c] | 1.86 | 67.45 | 7.68 | 95.25 | 0.761 | 1.146 |
| **MPt1**-ESY-SR101+GSH[c] | 1.99 | 61.95 | 7.97 | 94.32 | 1.099 | 1.221 |
| **MPt1**-ESY-SR101+Hcy[c] | 1.95 | 60.71 | 7.83 | 94.06 | 1.028 | 1.260 |

a: monitored at 500 nm upon excitation at 360 nm; [**MPt1**] = 10.0 $\mu$M, [ESY] = 0.18 $\mu$M.

b: monitored at 550 nm upon excitation at 360 nm; [**MPt1**] = 10.0 $\mu$M, [ESY] = 0.18 $\mu$M, [SR101] = 0.18 $\mu$M.

c: monitored at 606 nm upon excitation at 360 nm; [MPt1] = 10.0 μM, [ESY] = 0.18 $\mu$M, [SR101] = 0.18 $\mu$M. [Cys]=0.15 $\mu$M. [GSH]=0.15 $\mu$M. [Hcy]=0.15 $\mu$M.

Table S2. Fluorescence quantum yields of **MPt1**, **MPt1**-ESY, **MPt1**-ESY-SR101, $\beta$-CD@**MPt1**, $\beta$-CD@**MPt1**-ESY and $\beta$-CD@**MPt1**-ESY-SR101 in $H_2O/CH_3COCH_3$ (99:1, v/v).

| Sample | Concentration | Fluorescence quantum yields ($\Phi_f$)/% |
|---|---|---|
| **MPt1** | [**MPt1**] = 10.0 $\mu$M | 27.4 |
| **MPt1**-ESY | [**MPt1**] = 10.0 $\mu$M<br>[ESY] = 0.18 $\mu$M | 45.4 |
| **MPt1**-ESY-SR101 | [**MPt1**] = 10.0 $\mu$M<br>[ESY] = 0.18 $\mu$M<br>[SR101] = 0.18 $\mu$M | 55.9 |

Table S3. The energy transfer efficiency in $H_2O/ CH_3COCH_3$ (99:1, v/v).

| Sample | Concentration | energy transfer efficiency($\Phi_{ET}$) /% |
|---|---|---|
| **MPt1**-ESY<br>(100:1.8) | [**MPt1**] = 10.0 $\mu$M<br>[ESY] = 0.18 $\mu$M | 54.82 |
| **MPt1**-ESY-SR101<br>(100:1.8:1.8) | [**MPt1**] = 10.0 $\mu$M<br>[ESY] = 0.18 $\mu$M<br>[SR101] = 0.18 $\mu$M | 56.39 |

Table S4. Antenna effect. Antenna effect was the average value obtained by three parallel experiments.

| Sample | Concentration | Antenna effect |
|---|---|---|
| **MPt1**-ESY<br>(100:1.8) | [**MPt1**] = 10.0 $\mu$M<br>[ESY] = 0.18 $\mu$M | 11.42 |
| **MPt1**-ESY-SR101<br>(100:1.8:1.8) | [**MPt1**] = 10.0 $\mu$M<br>[ESY] = 0.18 $\mu$M<br>[SR101] = 0.18 $\mu$M | 16.07 |

Table S5. Summary of biothiols fluorescent probes described in this work.

| Probe name | Detection Type | $\lambda_{ex}/\lambda_{em}$ (nm) | LOD | Liner Range |
|---|---|---|---|---|
| **MPt1** assemblies | Turn off | 360/500 | Cys: $8.20 \times 10^{-8}$ M<br>GSH: $2.87 \times 10^{-7}$ M<br>Hcy:$1.01 \times 10^{-7}$ M | 0-0.5 $\mu$M |
| **MPt1**-ESY-SR101 assemblies | Turn off | 360/606 | Cys: $3.09 \times 10^{-8}$ M<br>GSH: $5.02 \times 10^{-8}$ M<br>Hcy: $5.05 \times 10^{-8}$ M | 0-1.0 μM |

## References


[1] X. Yan, H. Wang, C. E. Hauke, T. R. Cook, M. Wang, M. L. Saha, Z. Zhou, M. Zhang, X. Li, F. Huang, P. J. Stang, A suite of tetraphenylethylene-based discrete organoplatinum(II) metallacycles: controllable structure and stoichiometry, aggregation-induced emission, and nitroaromatics sensing, J. Am. Chem. Soc. **137** (2015) 15276−15286.

[2] M.G. Roberson, J.M. Duncan, K.J. Flieth, L.M. Geary, M.J. Tucker, Photo-initiated rupture of azobenzene micelles to enable the spectroscopic analysis of antimicrobial peptide dynamics, RSC. Adv, 10 (2020) 21464-21472.

[3] K. Wei, J. Li, G. Chen, M. Jiang, Dual molecular recognition leading to a protein–polymer conjugate and further self-assembly, ACS Macro Lett. 2 (2013) 278−283.